Research Article | Vol. 29, No. 5 / 1 March 2021 / Optics Express 7794
Optics EXPRESS

Balanced-detection interferometric cavity-assisted photothermal spectroscopy employing an all-fiber-coupled probe laser configuration

JOHANNES P. WACLAWEK,* HARALD MOSER, AND BERNHARD LENDL

Research Division of Environmental Analytics, Process Analytics and Sensors, Vienna University of Technology – TU Wien, Getreidemarkt 9/164, 1060 Vienna, Austria
johannes.waclawek@tuwien.ac.at

Abstract: The interferometric cavity-assisted photothermal spectroscopy (ICAPS) method has been proven highly suitable for sensitive and compact gas detection by application of an optical cavity as transducer for photothermal spectroscopy. This work reports on the implementation of an overall fiber-coupled probe laser configuration detecting the reflectance of the individual interferometers in a balanced-detection ICAPS system. The layout greatly improves the overall sensor system robustness. Two identical 1 mm path length cavities were used for balanced detection, enabling sensor operation close to the fundamental limit of shot noise by efficiently cancelling excess noise. A quantum cascade laser served as a mid-infrared excitation source to induce refractive index changes in the sample, and a near-infrared fiber laser served as probe source to monitor the photo-induced refractive index variations. The metrological figures of merit for the sensor were investigated by SO_2 detection. For the targeted absorption band centered at 1380.93 cm^{-1}, a 3 ppbv minimum detection limit was achieved with a 1 s integration time, corresponding to a normalized noise equivalent absorption of 4.5×10^{-9} cm^{-1} W $Hz^{-1/2}$.

1. Introduction

The selective quantification of various gas species at trace levels is critical in a variety of applications, including environmental monitoring, industrial process control, medical diagnostics, and scientific research [1–5]. Powerful laser based gas sensors have been developed, however, further advances in sensitive and rugged operation of miniaturized sensors are still needed. Such sensor miniaturization plays a crucial role in certain areas that require a small absorption volume or footprint, but still remains challenging to achieve. A small probe volume is beneficial for monitoring rapidly changing concentration levels in gas streams, due to the capacity for rapid gas exchange and thus fast sensor response, or simply for applications where only limited sample gas volumes are available. The well-established gas quantification methods based on direct absorption spectroscopy [2,3,5,6], however, show an inherently limited miniaturization potential due to the dependence of the sensitivity on the optical path length according to the Lambert-Beer law. In contrast, methods based on indirect absorption spectroscopy, such as photothermal spectroscopy (PTS) and photoacoustic spectroscopy (PAS), offer the potential for sensor miniaturization. Additionally, they feature the unique properties of a large dynamic range over a few orders of magnitude and a background-free sensor response [7–9]. These indirect methods detect changes in the sample's thermodynamic properties, probing variations in the refractive index (PTS) and acoustic waves (PAS), respectively. Indirect spectroscopic signals are

#416536 https://doi.org/10.1364/OE.416536
Journal © 2021 Received 7 Dec 2020; revised 22 Jan 2021; accepted 23 Jan 2021; published 26 Feb 2021

Optics EXPRESS

typically induced by an excitation laser. The absorption of electromagnetic waves by molecules excites their internal energy levels, which may lead to sample heating via energy transfer by collisional relaxation. A change in the sample's temperature causes a change in density and pressure, generating the PTS and PAS signals. The photo-induced signal is directly proportional to the temperature change within the excited sample volume, which in turn is directly proportional to the concentration and absorption coefficient of the absorbing molecules as well as to the incident laser power, and inversely proportional to the modulation frequency and cross-section of the excitation laser beam [7].

PTS sensing employing an interferometer as a transducer for monitoring photo-induced changes is a powerful approach for detection of trace gases [10–20]. Corresponding photothermal interferometry (PTI) setups employ an excitation laser for transient sample heating and a probe laser to monitor the resulting refractive index changes. Any change in the refractive index causes a phase shift of the electromagnetic waves passing through the heated region, which can be measured simply by detection of the probe laser intensity transmitted through the interferometer. Both, two-beam interferometers, such as the Mach-Zehnder [10–13] or Jamin [14] type, and multi-beam interferometers, such as the Fabry-Perot configuration [15–20], i.e., an optical cavity, have been applied to measure temperature-induced phase shifts. The fundamental sensitivity of a two-beam interferometer is dependent on the phase shift, whereas the sensitivity of a multi-beam interferometer is dependent on the phase shift as well as on the Finesse of the cavity, i.e., the reflectivity of its mirrors, each of which can be adjusted separately. Thus, the very simple configuration of the optical cavity enables the possibility for both highly sensitive and miniaturized transducers via a short interferometer spacing and moderately to highly reflective mirrors, as has been shown by *interferometric cavity-assisted photothermal spectroscopy* (ICAPS) [19,20]. The absence of any mechanical resonance allows the free selection of the modulation and hence the detection frequency. By this means, an optimum modulation frequency in terms of the maximum ratio of the photo-induced signal strength to noise can be selected, exploiting the inverse proportionality of indirect spectroscopy signals to modulation frequency. Moreover, the absence of any mechanic resonator renders frequent recalibration under changing environmental conditions unnecessary. The ICAPS sensing scheme has proven ability to provide white-noise-determined characteristics, resulting in excellent long-term stability due to feedback-controlled compensation of any transducer drifts [20]. This allows improvement of sensitivity by application of very long integration times, which may be of special interest for applications where the concentration of the target molecule changes either very slowly or not at all.

Any enhancement in sensitivity by an optical cavity, however, is only directly proportional to the point at which the source of limiting noise is not also proportionally enhanced. Limiting noise may be introduced via excess noise from the probe laser source, such as frequency and intensity noise, as well as environmental noise, such as sound. The susceptibility to excess noise is a potential drawback of the basic PTI scheme using an optical cavity [15–19]. However, excess noise in the signal path of a PTI setup can be efficiently removed by application of balanced-detection, splitting the probe beam into two equal parts for separate detection [20]. The subtraction of two detector signals allows rejection of common mode noise, i.e. noise that is present in both paths, down to the fundamental limit of shot noise [21–23]. The two-beam interferometer configuration enables rejection of common mode noise by application of balanced detection simply by using the two complementary output branches [14]. When applying an optical cavity as transducer, efficient rejection of common mode noise requires balanced detection via two cavities [20]. An important aspect in this regard is that identical characteristics of the two cavities are essential in order to yield the same excess noise response in both probe channels. Identical characteristics include identical optical and mechanical configurations as well as presence of the same sample gas with the same properties, such as composition, pressure, and temperature. This is of particular relevance when rapid changes may occur in the target

Optics EXPRESS

molecule and/or matrix. Balanced detection not only improves the sensitivity of a given ICAPS setup by enhancing the signal-to-noise ratio but also increases the ruggedness of the sensor by enhancing the immunity to external disturbances. Therefore, balanced-detection ICAPS links the general advantages of the optical cavity as the transducer of the PTI method with the advantages of balanced detection and its shot-noise-limited properties.

This work reports on the implementation of an all-fiber-coupled probe laser configuration in the balanced-detection ICAPS system, probing the reflectance of the individual interferometers. The use of optical fibers together with probing the reflectance greatly improves the sensor ruggedness by avoiding free-space probe laser beams and by precluding any possible mismatch in the beam guiding at the interferometer coupling/collecting interface. Refractive index changes induced by the excitation laser were monitored by a sample probe laser transversely intersecting the excitation beam. This layout offers simple beam alignment and avoids any heating of the interferometer mirrors by the excitation beam, which could disturb the signal, thus enabling a simple, robust, and compact gas sensor design. High sensitivity was accomplished by application of interferometers with moderate finesse as well as a small mirror spacing of 1 mm together with strong photo-thermal signal generation by use of high excitation laser intensities. Transient generation of the photothermal signals was performed by applying wavelength modulation (WM) at reduced sample pressure via a powerful continuous wave (CW) distributed feedback (DFB) quantum cascade laser (QCL) as excitation source to target strong fundamental absorption features of the sample molecules in the mid-infrared (mid-IR) region. The photo-induced transducer signal was detected within a narrow bandwidth by a lock-in amplifier (LIA) at the second harmonic ($2f$) of the modulation frequency [24]. This $2f$-WM scheme is a powerful method for increasing the signal-to-noise ratio as well as the selectivity of a given measurement. Refractive index changes were detected via a CW-DFB fiber laser (FL) emitting in the vicinity of 1550 nm together with a photodiode. This near-infrared region offers mature technology and readily available high-performing optical components. The metrological figures of merit of this $2f$-WM balanced-detection ICAPS sensor employing an all-fiber-coupled probe laser configuration were investigated using sulfur dioxide (SO_2) as the target molecule.

2. Basic sensor operation principle, sources of noise, balanced detection, and sensor architecture

2.1. Basic sensor operation principle

A Fabry-Perot interferometer (FPI), i.e. an optical cavity, can be used to detect changes in the refractive index of a gaseous sample with high sensitivity by monitoring the phase shift of electromagnetic radiation passing through the device. Changes in the refractive index of the sample can be induced via the photothermal effect, whereby an induced temperature change alters the sample density [7]. An FPI simply consists of two partially transmitting mirrors spaced at a certain distance [see Fig. 1(a)]. Radiation entering the FPI is partially reflected by the input mirror. The transmitted intensity portion is further reflected between the two mirrors, forming an infinite series of partial waves in forward and backward direction. With each reflection, intensity is coupled out of the FPI in both directions. The periodic transmission, or resonances, of an ideal FPI is described by the Airy function [25,26], whose characteristic is dependent on the finesse of the optical cavity and on the phase difference for a cavity round trip. The finesse is only determined by the reflectivity of the two mirrors, whereas the phase difference is dependent on the vacuum wavelength, the angle of incidence, the spacing of the mirrors, and the refractive index of the medium between the mirrors. At the resonance frequencies, the transmittance of the cavity is maximized, while its reflectance is minimized [see Figs. 1(b) and 1(c)]. The beam that is transmitted through the FPI is the leakage beam, which is the part of the standing wave inside the cavity that leaks out of the second mirror. The reflected beam, however, is the sum of two different beams: The part that is promptly reflected by the first mirror and the part that is leaking

Optics EXPRESS

out of the cavity through the first mirror traveling in backward direction. The relative phase of these two parts strongly depend on the laser frequency. If the laser frequency is perfectly matched to one resonance frequency of the cavity, the promptly reflected beam and the leakage beam are exactly 180 degrees out of phase, resulting in destructive interference. Any deviation from resonance will cause the phase difference to deviate from 180 degrees, and thus from complete destructive interference. The forward transmittance as well as the backward reflectance can be employed to detect changes in the refractive index of the gas inside the FPI. Detection of the forward transmitted beam has been shown in [15,16,19,20]; this work demonstrates detection of the reflected beam. One advantage of detection of the cavity's reflectance is the increased robustness in beam coupling to the optical detector. Here, the same optical part that is used to couple the laser beam into the FPI is also used to collect the beam reflected by the cavity. By this means, no additional optical part for collection of the transmitted beam on the output mirror of the FPI has to be used, making the system more rugged simply by avoiding any possible coupling mismatch.

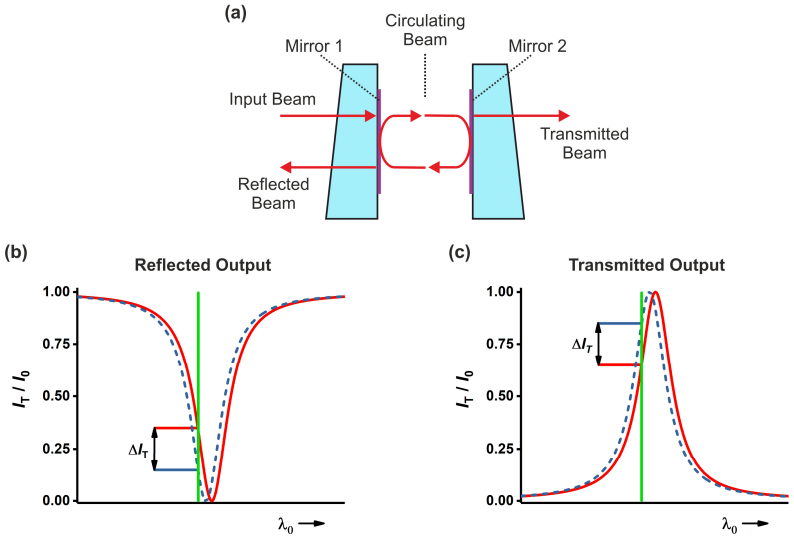

Fig. 1. (a) Schematic of the Fabry-Perot interferometer. ICAPS operation principle for (b) the reflected intensity, and (c) the transmitted intensity; in both cases, the frequency of a probe laser (green line) is tuned near the inflection point on one side of the cavity's resonance, incorporating sample gas at thermal equilibrium (red trace). Photo-induced heating of the sample by an excitation laser decreases the sample's refractive index, which is accompanied by a shift in the transmittance and reflectance with respect to the vacuum wavelength (blue dotted trace). This shift is monitored by a photodiode via a change in the detected probe laser intensity (ΔI_T).

The ICAPS operation principle is essentially the same for the detection of both transmittance and reflectance. The periodic transmission of the interferometer is shifted with respect to the vacuum wavelength when the refractive index of the sample between the two mirrors changes due to photothermal heating [Figs. 1(b) and 1(c)]. This shift is monitored via a photodiode as a change in the transmitted intensity, using a probe laser that is tuned to a frequency enabling partial transmission/reflectance. The highest sensitivity to variations in the phase difference is found near the inflection point on one side of the periodic resonances, at approximately 25% of the height of the function for reflectance and 75% for the transmittance, respectively. At this point, the slope of the function is at its maximum and is roughly linear over a narrow range, yielding a linear sensor response to induced temperature changes.

Optics EXPRESS

2.2. Sources of noise and balanced detection

The principal sources of noise in an ICAPS system are excess probe laser noise and environmental noise. Excess probe laser noise arises from frequency and intensity fluctuations of the emitted probe laser radiation, the characteristics of which depend on the type of laser used [27]. Environmental noise may be introduced by acoustic and mechanical perturbations, which may induce on the one hand variations in the refractive index of the media inside the cavity due to pressure changes, and on the other hand minute variations in the cavity geometry, both of which affect the transmission function characteristics. In addition, the driving conditions of the probe laser source influence noise content, e.g., lower driving currents may yield higher intensity noise, while a noisy driving source will translate directly into enhanced frequency noise. Any noise is ultimately detected by the photodiode as intensity fluctuation (see Fig. 2). Frequency noise as well as environmental noise will be enhanced proportionally to the slope of the periodic transmission of the cavity. Intensity noise will not be affected by the cavity properties, as it is only a measure of the probe laser.

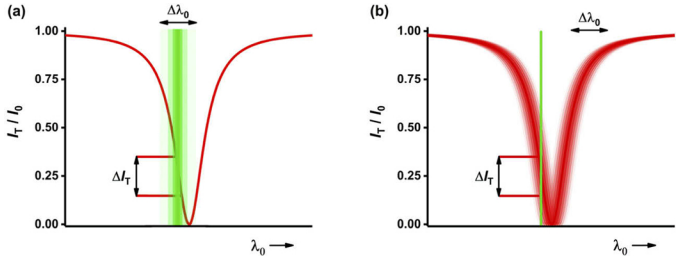

Fig. 2. Schematic illustration of different excess noise sources of an ICAPS setup: (a) probe laser noise (frequency fluctuations), and (b) environmental noise (e.g. sound).

An improvement in terms of sensitivity as well as robustness of an ICAPS system is obtained by cancellation of excess noise down to the fundamental limit of shot noise via employment of a balanced-detection scheme. Within this scheme excess noise can be removed with high efficiency, by simultaneously comparing the probe laser's intensity with and without the photo- thermal signal. The concept of balanced-detection ICAPS (BICAPS) in an all-fiber coupled probe laser configuration detecting the photothermal signal via reflectance is schematically depicted in Fig. 3. The fiber-coupled probe beam is split by a beam splitter into two equal beams – a sample probe beam and a reference probe beam. The beams are then coupled into two separate cavities (a sample and reference cavity), having identical properties within the gas cell. The sample probe beam intersects the excitation beam and propagates through the photo-induced heated region of the sample. The signal of the sample probe beam carries the photothermal signal, which is superimposed by noise. In contrast, the reference probe beam only probes noise due to the lack of any photothermal excitation. The reflectance of the interferometers is detected by two separate photodiodes. The backward traveling light is collected by the collimator and separated from the forward traveling light coming from the laser source via an optical circulator. The signals of the two photodiodes are subtracted by a differential amplifier, enabling cancellation of identical noise present in both parts with high rejection ratio.

2.3. Sensor architecture

The architecture of the all-fiber-coupled probe laser 2f-WM balanced-detection ICAPS based gas sensor is schematically depicted in Fig. 4(a). This setup uses two separate optical cavities with identical properties. The air-spaced etalons consist of two fused silica plates ($10 \times 5 \times 2$ mm) on which dielectric-coated mirrors with reflectivity of $R = 0.989$ are deposited, yielding an

Optics EXPRESS

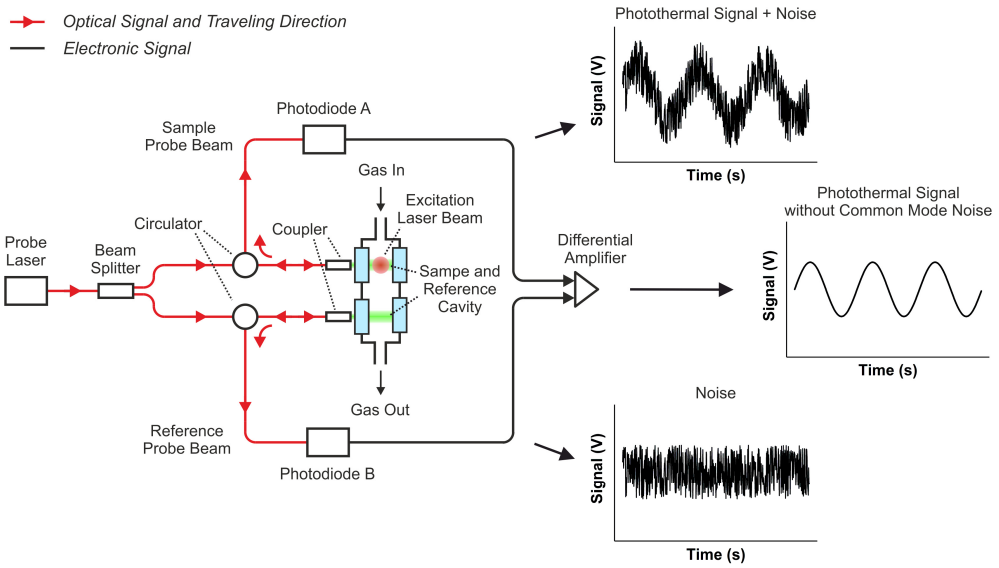

Fig. 3. Principle of balanced-detection ICAPS monitoring the reflectance of the interferometers in an all-fiber-coupled probe laser configuration; the probe beam is split into two equal parts – a sample probe beam and a reference probe beam – and coupled by a collimator into two separate but identical interferometers. The sample beam probes the photothermal signal, which is superimposed by noise, whereas the reference beam probes only noise. The reflected light is again collected by the coupler and separated from the forward propagating light coming from the probe laser by a circulator, routing the beam to a photodiode. By subtraction of the two photodiode signals, the photothermal signal is received along with high rejection of common mode noise.

effective finesse of approximately 90. In each case the cavity mirrors are fixed to each other by spacers of 1 mm thickness [see Fig. 4(c)]. One cavity was used as the transducer for monitoring induced changes in the refractive index [see Fig. 4(b)], while the second cavity was used to apply balanced detection. Photothermal-induced refractive index changes inside the sample cavity were monitored via a fiber-coupled, single-mode tunable CW-DFB-FL (probe laser). The probe laser emitted a beam at a wavelength of ~1550 nm with a constant optical output power of 40 mW; its wavelength could be thermally tuned within a total range of ~1.2 nm. The output of the fiber of the probe laser was connected to a fiber-optic beam splitter, splitting the beam into two parts of equal power (50:50). The two beams were routed through fiber-coupled optic circulators whose corresponding ports were coupled to a pigtailed gradient-index (GRIN) fiber-optic collimator (working distance, WD = 15 mm, beam diameter at WD = 0.5 mm FWHM). These collimators served to couple the forward traveling light into the corresponding cavity and the backward travelling light again into the fiber. The reflected light was separated from the forward traveling light by a circulator and sent to a photodetector consisting of a gallium indium arsenide (GaInAs) positive intrinsic negative junction (PIN) photodiode amplifying the signal via a trans-impedance amplifier (TIA). The intensities of these individually reflected beams were adjusted by fiber-coupled attenuators ahead of the detectors to avoid saturation, whereby an optical power of ~1.9 mW impinged on each photodiode. All probe laser beams were thus guided in optical fibers. The parts of the two beams transmitting through the cavities in the forward direction were simply absorbed by a beam dump outside of the measuring cell. The electronic outputs of the photodiodes were passed to a 4^{th} order Gaussian high-pass filter with a

Optics EXPRESS

3 dB cut-off frequency of 200 Hz and a low-noise differential amplifier with a gain of 100, whose output was fed into a lock-in amplifier (LIA). The probe laser emission frequency was maintained at the operation point of the sample cavities' transmission function via a slow feedback circuit (mHz), by using the DC component of the photodetector, which monitored the sample probe beam's reflected intensity (photodetector A). By controlling the DC-component, any drift of the transducer, e.g., due to temperature or changing sample gas composition, or drift of the emitted laser frequency itself was automatically compensated. The operation point of the reference interferometer was kept at the probe laser's emission frequency by monitoring the reflected reference probe beam intensity of the reference cavity (photodetector B) and by controlling the temperature of the measurement cell. This allowed fine adjustment of the interferometer spacing, again using a slow feedback circuit (mHz). By using two independent feedback circuits, the probe laser was locked to the inflection point of the sample cavity, while the transmission functions of the two cavities were locked to the same frequency. This yielded the same response to noise in both channels, thus enabling efficient noise rejection. The interferometer's substrates were fixed into a compact and gas-tight aluminum cell. Transmission of the probe laser beams was enabled directly by the interferometer substrates and two fused silica windows, respectively, transmission of the QCL beam through the cell was enabled by two CaF_2 windows. Sample gas exchange was performed via gas in- and outlets. The outer dimensions of the cell were $40 \times 30 \times 30$ mm with a total inner sample gas volume of a few cm⊃3. The layout of the photothermal signal generation and processing was equivalent to that described in Ref. [20]: Selective heating of the sample gas inside the interferometer was performed by using a collimated, high heat load (HHL) packaged CW-DFB-QCL emitting at a wavelength of 7.25 µm (excitation laser), whose frequency could be tuned by varying the QCL temperature via injection current and temperature control by a Peltier element. The QCL output beam was focused by a plano-convex CaF_2 lens ($f = 50$ mm) between the two mirrors forming the sample cavity to induce strong photothermal excitation via the high laser intensity, intersecting the standing wave of the sample probe beam in the transverse direction. Focusing the QCL beam yielded a calculated Gaussian beam waist diameter of about 140 µm. The sensor platform was based on photothermal sample excitation via wavelength modulation and detection of the second harmonic ($2f$) by demodulation of the alternating current (AC) component of the differentially amplified photodetector signals, i.e., the balanced signal, using an LIA. The digitized electronic signals were transferred to a computer for further data processing in a LabVIEW-based program. The QCL beam was additionally guided after transmission through the measurement cell into a reference cell filled with SO_2 in N_2 at an absolute pressure of 133 mbar, and finally onto a pyroelectric photodetector. The reference gas cell and the photodetector were used as the reference channel for an optional lock of the QCL frequency to the center of the selected SO_2 absorption line using the $3f$ LIA output, preventing long-term drift of the QCL frequency. To do this, the direct current (DC) component of the QCL driver was adjusted proportionally via electronic feedback control to maintain its emission at the desired frequency. To implement the WM technique, the emission wavelength of the QCL was modulated by adding a sinusoidal function to the DC injection current input. The detected sample probe beam intensity was modulated when the temperature of the gas inside the sample cavity was altered via absorption of the excitation laser radiation by the target molecules. The ICAPS detection was performed in two different modes: Scan and locked mode. In the scan mode, spectra of the sample gas were acquired by slowly tuning (mHz) the QCL frequency over the desired spectral range around the target absorption line through a change of the DC injection current component using a sawtooth function. In the locked mode, the QCL frequency was locked to the center of the selected SO_2 absorption line, ensuring stable long-term measurements. The pressure and flow of the sample gas inside the measurement cell were controlled and maintained by using a metering valve, pressure sensor, pressure controller, and mini diaphragm vacuum pump. The metrological figures of merit for the presented sensor were investigated by employing

Optics EXPRESS

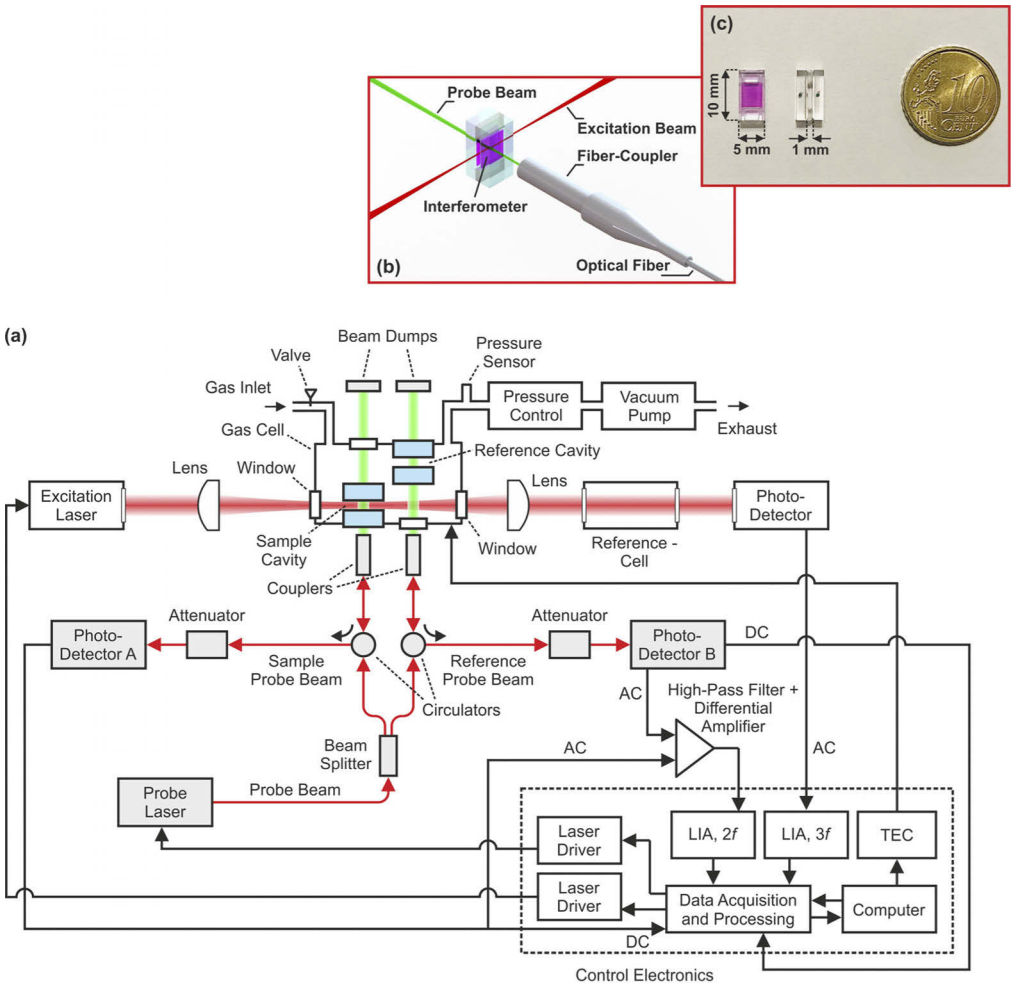

Fig. 4. (a) Schematic of the balanced-detection ICAPS based gas sensor employing an all-fiber-coupled probe laser configuration, monitoring the reflectance of the interferometers. (b) Illustration of the ICAPS principle, (c) Photograph of the employed interferometers (top and side view) having a mirror spacing of 1 mm in comparison with a 10 eurocent coin for scale.

a modulation frequency of $f_{\mathrm{mod}} = 297$ Hz, a modulation depth of $\Delta\nu = \pm 0.09$ cm^{-1}, an LIA time constant set to $\tau = 1$ s, and a sawtooth excitation laser tuning frequency of $f = 6.67$ mHz. The absolute pressure and flow of the sample gas was kept constant at $p = 200$ mbar and $u = 25$ mL min^{-1}.

3. Experimental

3.1. Investigation of noise cancellation performance via balanced detection

To investigate the possible signal-to-noise ratio improvement of the balanced-detection ICPAS scheme, noise power spectra of the photodiodes' response at the output of the differential amplifier were recorded using a spectrum analyzer. Spectra taken with of two different setup configurations were analyzed: First, the noise power spectrum of direct illumination onto the photodiodes, without any cavity, was recorded. This setup was simply composed of the two

Optics EXPRESS

photodetectors and the equally split probe laser beams. To ensure equivalent power impinging on the detectors, reprehensive of the reflectance from the cavities in the ICAPS system, the power of the individual paths was adjusted by attenuators ahead of the detectors. By recording the spectrum once for non-balanced-detection and once for balanced detection, the shot noise level of the probe laser–detector system could be determined experimentally [21], excluding potential noise contribution from the cavities. Moreover, to verify dependence of the noise behavior on the probe laser operation parameters, the non-balanced-detection spectra for two different laser-driving conditions were recorded. Second, the noise power spectra of the ICAPS sensor for the basic (non-balanced) and balanced-detection configuration were recorded, at total pressure of 200 mbar and flushing the cell with pure N_2. The setup shown in Fig. 4(a) was used, except that the output of the differential amplifier was routed to the spectrum analyzer instead of feeding to the LIA.

The results of the measurements are plotted in Fig. 5 for a frequency range from 0 to 2.5 kHz [Fig. 5(a)] and from 0 to 10 kHz [Fig. 5(b)]. The theoretical shot noise level of this setup was calculated to be −105 dB. The recorded noise level for balanced-detection of the direct photodiode illumination is in good agreement with the calculated shot noise level above 5 kHz. The noise level in the frequency range below 5 kHz is slightly above the theoretical shot noise level, following the typical characteristics on $1/f$ noise influence in this frequency regime. The steep decline of the traces for direct illumination in the frequency regime <1.5 kHz is caused by a combination of the characteristics of the probe laser itself and a measurement artifact caused by the differential amplifier and the low-impedance input of the spectrum analyzer. The comparison of the noise power spectra for direct photodiode illumination (purple, red, and blue traces) show a maximum possible improvement in the noise level by balanced-detection at the selected $2f$-WM detection frequency around 600 Hz of ~28.5 dB (factor 27) for operation of the probe laser with minimal driving current and ~20.8 dB (factor 11) for operation with maximum driving current. The noise reduction potential improves with increasing frequency from ~20.8 dB (factor 11) at 600 Hz to ~30 dB (factor 32) at 10 kHz for operation of the probe laser with maximum driving current.

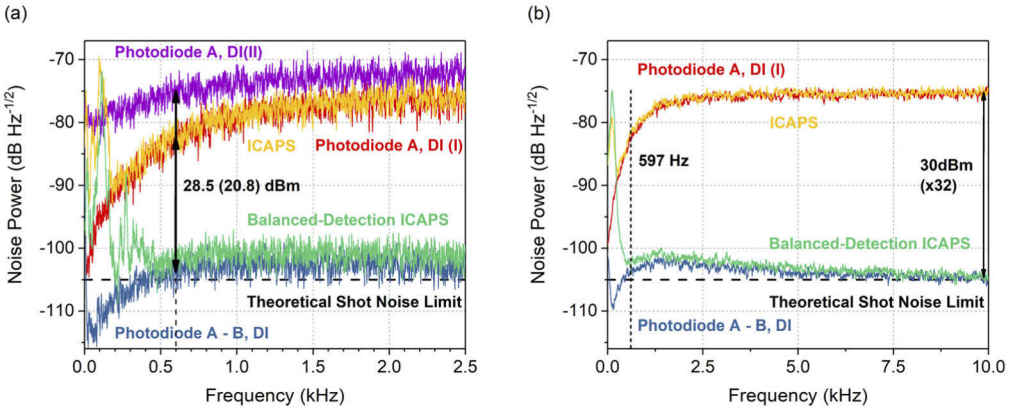

Fig. 5. Noise power spectrum for the basic, non-balanced ICAPS (orange traces) and balanced-detection ICAPS configuration (green traces), in comparison to direct illumination (DI) of the photodiodes with two different driving conditions for non-balanced (red traces, purple trace) and balanced detection (blue traces); (a) most relevant frequency range from 0 to 2.5 kHz for photothermal signal generation, showing the potential improvement using balanced detection around 600 Hz, and (b) for a wider bandwidth of 10 kHz.

Comparison of the recorded noise spectra of the ICAPS setup to the direct illumination setup show excellent accordance for non-balanced detection and very good accordance for

Optics EXPRESS

balanced-detection above 500 Hz. The noise power spectra of the ICAPS setup show elevated noise levels below the 500 Hz regime. This behavior is most likely caused by noise introduced by the cavities. At the detection frequency of 600 Hz the balanced-detection ICAPS setup show a slightly elevated noise floor of 2.2 dB (factor 1.3) in comparison to the balance of direct illumination. This small discrepancy from optimum noise-cancelling performance of balanced-detection ICAPS to balanced-detection of direct photodiode illumination (green vs. blue trace) above 500 Hz is caused by a little imbalance within the sample and reference path of the ICAPS system, i.e., a minor voltage level and noise response difference within the two detector channels.

To analyze the measured results of the spectrum analyzer having a low impedance input and thereof distorting the signals in the low frequency range, the noise of the system was investigated in the detection frequency range from 0 to 10 kHz by recording the LIA output having a high impedance input of 10 MHz, with a time constant of t = 100 ms and a 18 dB/oct low pass filter setting. Figure 6 shows the measurement results for three different measurement configurations at different frequencies: non-balanced and balanced detection of direct photodiode illumination, and balanced-detection ICAPS using the setup as shown in Fig. 4(a). Each plotted datapoint represents the average collected over 20 min. The level of the shot noise was assumed to be at the same level as for balanced detection of direct illumination of the photodiodes at 10 kHz [see Fig. 5(b)]. The improvement in noise for direct illumination employing balanced-detection at the 2*f* detection frequency of 600 Hz is about 21.2 dB (factor 12) and for balanced-detection ICAPS about 19 dB (factor 9), which is in excellent agreement with the data recorded with the spectrum analyzer. Again, comparison of the two values for the different balanced-detection setups shows only a 2.2 dB (factor 1.3) elevation of the noise floor around 600 Hz for the ICAPS system compared to the ideal balance conditions. In contrast to the measurement with the spectrum analyzer, a clear increase in noise below the 500 Hz regime can be observed. This behavior can be attributed to the typical 1/*f* noise of electronic systems. Exceedingly high noise can be observed at frequencies below 150 Hz for balanced-detection ICPAS, as was also recorded by the spectrum analyzer. In contrast to the measurement of the spectrum analyzer, the noise of the non-balanced direct illumination configuration first drops and then increases to a plateau with increasing frequency. This behavior is most likely due to noise behavior of the laser, which decreases with decreasing frequency, and the overlap with the 1/*f* noise of the system.

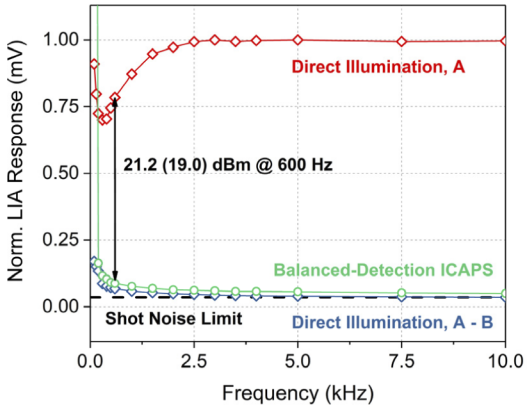

Fig. 6. Measured LIA response of the noise for non-balanced and balanced detection of the photodiodes under direct illumination, as well as the noise of the all-fiber probe laser coupled balanced-detection ICAPS system detecting the reflectance for a frequency range of 10 kHz.

Optics EXPRESS

In summary, the two different noise measurement methods (spectrum analyzer and LIA) reveal operation of the balanced-detection ICAPS system close to the fundamental limit of shot noise above detection frequencies of 500 Hz.

3.2. Investigation of the signal-to-noise ratio

To identify the optimum modulation/detection frequency of the ICAPS system in terms of highest signal-to-noise ratio, the sensor response was recorded for a concentration of 1 ppmv SO_2 at 200 mbar at different frequencies within a bandwidth of 10 kHz. The sensor was operated in the locked mode and the data each frequency were recorded for a total duration of 5 min and averaged. The results of the measured response showing flattening with decreasing frequency mainly caused by the used high-pass filter are shown in Fig. 7(a), along with the theoretical signal behavior having an inverse proportionality to the modulation frequency [7]. To obtain the signal-to-noise ratio for the ICAPS system, these data were divided by the recorded noise for balanced detection shown in Fig. 6 (green trace). The highest signal-to-noise ratio was found around the 2f detection frequency of 300 Hz [Fig. 7(b)]. To facilitate comparison to previous publications, the modulation frequency of 297 Hz, i.e., 2f detection frequency of 594 Hz, was used for further measurements even though it showed an ~1.25 times decrease in the signal-to-noise ratio.

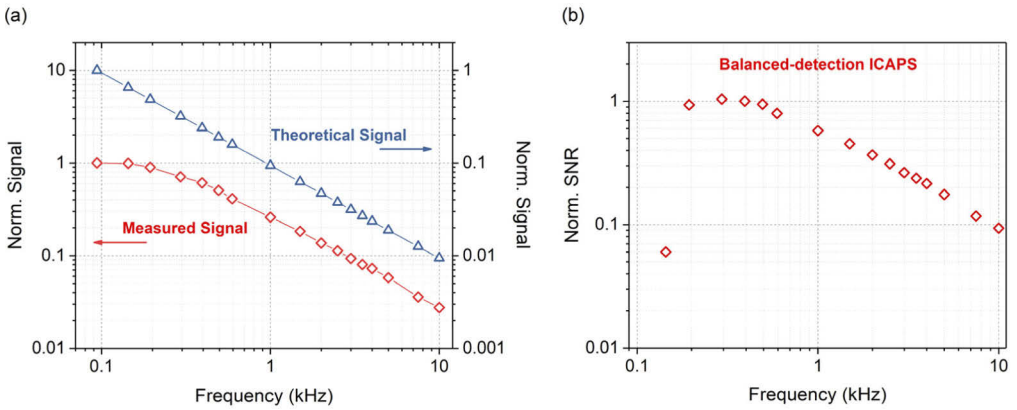

Fig. 7. (a) Normalized sensor response of the balanced-detection ICAPS system for a concentration of 1 ppmv SO_2 versus theoretical behavior at different 2f-WM detection frequencies; (b) balanced-detection ICAPS sensor signal-to-noise ratio.

3.3. Selectivity, sensitivity, and linear response of the sensor

To investigate the metrological figures of merit for the sensor, sulfur dioxide (SO_2), which has strong and separated absorptions within the spectral region covered by the employed QCL, was used as the target molecule. The absorption band centered at 1380.93 cm^{-1} [28], which is situated within the ν_3 fundamental spectral range, was selected for photothermal excitation. Different trace gas concentration levels were obtained by blending a 1 ppmv SO_2 calibration mixture with N_2 via a custom gas mixing system. Here, the combination of two mass flow controllers with different flow ranges, having a specified accuracy of ± 0.3% of the full scale of the gas flow range, allowed a dynamic mixing ratio of up to 1:1000.

The selective response of the balanced-detection ICPAS sensor to various concentrations of SO_2 in N_2 was verified by recording 2f-WM spectra for three different trace gas levels (200, 400, and 1000 parts per billion by volume, ppbv) as well as the noise floor of the sensor for pure N_2 [see Fig. 8(a)]. The spectra were achieved by slowly tuning the QCL wavelength by a few mHz

Optics EXPRESS

across the selected SO_2 absorption band centered at 1380.93 cm^{-1}. Sensitivity and linearity of the sensor response to SO_2 traces were determined by continuous monitoring of different concentration levels within the range of 0 to 1000 ppbv utilizing the locked mode with the QCL frequency fixed to the center of the selected SO_2 absorption line by means of the reference path. The 2*f*-WM signals were acquired for a total duration of 10 min for each concentration level. The signal acquisition was stopped for 1 min when the SO_2 concentration was changed to allow the concentration to stabilize. The results of the stepwise measurement are shown in Fig. 8(b). Averaging of the data for each concentration step yielded excellent linearity between the measured signal amplitudes and the SO_2 concentrations [see inset of Fig. 8(b)]. Based on the averaged signal amplitudes for 200 ppbv SO_2 and the standard deviation of the noise level for pure N_2, a signal-to-noise ratio of ~70 was calculated, which yielded a 1σ minimum detection limit (MDL) of 3 ppbv for an acquisition time of 1 s. The measured optical power emitted by the QCL directly at the HHL output at the frequency of the selected SO_2 absorption band centered at 1380.93 cm^{-1} was approximately 203 mW ($T = 279.15$ K, $I = 398$ mA). The QCL beam was focused through

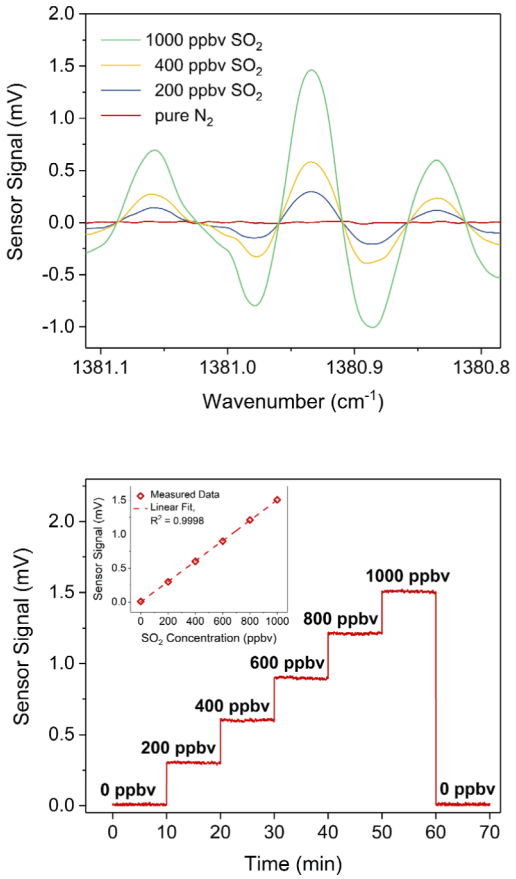

Fig. 8. (a) 2*f*-WM balanced-detection ICAPS sensor response for three different sample gas concentrations as well as the sensor noise floor for pure N_2, recorded when the QCL frequency was tuned over the targeted absorption band centered at 1380.93 cm^{-1} at an absolute pressure of 200 mbar. (b) Consecutive monitoring of increasing SO_2 concentration steps, together with the sensor noise for balanced-detection ICAPS (pure N_2); the inset reveals the highly linear performance of the sensor response to varying sample gas concentration levels.

Optics EXPRESS

the sample cavity with high transmission efficiency, yielding an optical power of ~174 mW in between the interferometer to interact with the sample gas, after accounting for absorption losses of the lens and one window of the gas cell. The normalized noise equivalent absorption (NNEA) coefficient at unit laser power and bandwidth was calculated to be NNEA = 4.5×10^{-9} cm^{-1} W Hz$^{-1/2}$, using a minimum detectable SO_2 absorption coefficient of $\alpha_{min} = 7.92 \times 10^{-9}$ cm^{-1}, an optical excitation power of $P = 174$ mW, and an LIA detector bandwidth of $\Delta f = 94$ mHz ($\tau = 1$ s, 18 dB/oct low-pass filter).

4. Conclusions and outlook

The work presented demonstrates highly sensitive, compact, and robust trace-gas sensing by balanced-detection ICAPS with the new implementation of an all-fiber-coupled probe laser configuration and detection of the interferometers reflectance. The capabilities of the method were demonstrated on the example of SO_2 detection down to the single-digit ppbv concentration range by employing two separate optical cavities with a mirror spacing of 1 mm together with a mid-infrared CW-DFB-QCL as the excitation source. The improvement of this setup compared to the previously published balanced-detection ICAPS method [20] is addressed by the inclusion of the fiber-coupled probe laser setup configuration and detection of the reflected signal. This implementation increases sensor robustness significantly by eliminating free-space optics in the probe beam path, and furthermore results in a greatly simplified handling of the system. Moreover, detection of the reflectance eliminates any mismatch in the beam guiding of the coupling-collecting/interferometer interface, enabling collection of the interferometer signal without a misalignment simply by the use of a single optical component together with the cavity. In addition, the circulator also acts as an isolator, minimizing back-reflections to the probe laser source. This advance makes significant progress towards a reliable industry-ready ICAPS system. The application of balanced detection improves the sensitivity by enhancing the signal-to-noise ratio, while the ruggedness of the ICAPS method is improved due to decreased interference of environmental noise. The ability to significantly improve the analytical figures of merit of the described balanced-detection scheme is demonstrated by achieving excellent common mode noise cancellation, resulting in an improvement of 19 dB (factor 9), as well as in a sensor noise floor minor above the limit of shot noise level (2.2 dB, factor 1.3). The MDL was determined to be 3 ppbv SO_2 employing a 1 s integration time, which yields a corresponding NNEA of 4.5×10^{-9} cm^{-1} W Hz$^{-1/2}$. The presented sensor is based on a compact arrangement with a detection volume of only a few cm⊃3. The principal concept of this sensor, however, shows high potential for further miniaturization, even down to integration on a chip. Since the ICAPS technique is based on indirect detection, it can detect any modulated changes of the refractive index of the sample. As such, this method is not limited to a particular excitation wavelength range but can be applied to a broad range of excitation sources. Also, more than one excitation source may be coupled to the transducer, allowing for multi-component analysis. Additionally, the robust transducer element also allows for high temperature and pressure applications. Future improvements in terms of sensitivity of the ICAPS setup can include the use of a steeper interferometer resonance, e.g., by use of a cavity with higher finesse, to probe stronger photothermal signals. In this regard, the balanced-detection scheme is a key aspect of this sensor principle. It allows for improving the sensitivity via an increase in the cavity finesse, thereby preventing any proportional enhancement in the noise, due to the efficient common mode noise rejection. This property is especially true for laser frequency and environmental noise, which will become more dominant at higher finesse values. In addition, the implementation of a further optical cavity to enhance the excitation laser power will raise the sensitivity by proportionally enhancing the photothermal-induced signal. An improvement in the detection limit can be achieved by exploiting the white-noise characteristics

Optics EXPRESS

of the balanced-detection ICAPS scheme for long-term signal averaging over a few thousand seconds.

Funding. Austrian Science Fund (PIR 40-N34); Austrian Research Promotion Agency (MIRCAVS 856914).

Disclosures. The authors declare no conflicts of interest.

References

1. F. K. Tittel, D. Richter, and A. Fried, "Mid-infrared laser applications in spectroscopy," Topics in App. Phys. **89**, 458–529 (2003).
2. U. Willer, M. Saraji, A. Khorsandi, P. Geiser, and W. Schade, "Near- and mid-infrared laser monitoring of industrial processes, environment and security applications," Opt. Laser Eng. **44**(7), 699–710 (2006).
3. H. Moser, W. Pölz, J. P. Waclawek, J. Ofner, and B. Lendl, "Implementation of a quantum cascade laser-based gas sensor prototype for sub-ppmv H_2S measurements in a petrochemical process gas stream," Anal. Bioanal. Chem. **409**(3), 729–739 (2017).
4. A. Amann, W. Miekisch, J. Schubert, B. Buszewski, T. Ligor, T. Jezierski, J. Pleil, and T. Risby, "Analysis of exhaled breath for disease detection," Annu. Rev. Anal. Chem. **7**(1), 455–482 (2014).
5. J. Hodgkinson and R. P. Tatam, "Optical gas sensing: A review," Meas. Sci. Technol. **24**(1), 012004 (2013).
6. J. B. McManus, M. S. Zahniser, D. D. Nelson, J. H. Shorter, S. C. Herndon, D. Jervis, M. Agnese, R. McGovern, T. I. Yacovitch, and J. R. Roscioli, "Recent progress in laser-based trace gas instruments: Performance and noise analysis," Appl. Phys. B **119**(1), 203–218 (2015).
7. S. E. Bialkowski, N. G. C. Astrath, and M. A. Proskurnin, *Photothermal Spectroscopy Methods*, 2nd Edition (John Wiley & Sons, 2019).
8. A. Miklós, P. Hess, and Z. Bozóki, "Application of acoustic resonators in photoacoustic trace gas analysis and metrology," Rev. Sci. Instrum. **72**(4), 1937–1955 (2001).
9. R. F. Curl, F. Capasso, C. Gmachl, A. A. Kosterev, J. B. McManus, R. Lewicki, M. Pusharsky, G. Wysocki, and F. K. Tittel, "Quantum cascade lasers in chemical physics," Chem. Phy. Lett. **487**(1-3), 1–18 (2010).
10. C. C. Davis and S. J. Petuchowski, "Phase fluctuation optical heterodyne spectroscopy of gases," Appl. Opt. **20**(14), 2539–2554 (1981).
11. W. Jin, Y. Cao, F. Yang, and H. L. Ho, "Ultra-sensitive all-fibre photothermal spectroscopy with large dynamic range," Nat. Commun. **6**(1), 6767 (2015).
12. Z. Li, Z. Wang, F. Yang, W. Jin, and W. Ren, "Mid-infrared fiber-optic photothermal interferometry," Opt. Lett. **42**(18), 3718–3721 (2017).
13. C. Yao, Q. Wang, Y. Lin, W. Jin, L. Xiao, S. Gao, Y. Wang, P. Wang, and W. Ren, "Photothermal CO detection in a hollow-core negative curvature fiber," Opt. Lett. **44**(16), 4048–4051 (2019).
14. D. L. Mazzoni and C. C. Davis, "Trace detection of hydrazines by optical homodyne interferometry," Appl. Opt. **30**(7), 756–764 (1991).
15. A. J. Campillo, S. J. Petuchowski, C. C. Davis, and H.-B. Lin, "Fabry-Perot photothermal trace detection," Appl. Phys. Lett. **41**(4), 327–329 (1982).
16. B. C. Yip and E. S. Yeung, "Wavelength modulated Fabry-Perot interferometry for quantitation of trace gas components," Anal. Chim. Acta **169**, 385–389 (1985).
17. F. Yang, Y. Tan, W. Jin, Y. Lin, Y. Qi, and H. L. Ho, "Hollow-core fiber Fabry-Perot photothermal gas sensor," Opt. Lett. **41**(13), 3025–3028 (2016).
18. K. Krzempek, G. Dudzik, and K. Abramski, "Photothermal spectroscopy of CO_2 in an intracavity mode-locked fiber laser configuration," Opt. Express **26**(22), 28861–28871 (2018).
19. J. P. Waclawek, V. C. Bauer, H. Moser, and B. Lendl, "2f-wavelength modulation Fabry-Perot photothermal interferometry," Opt. Express **24**(25), 28958–28967 (2016).
20. J. P. Waclawek, C. Kristament, H. Moser, and B. Lendl, "Balanced-detection interferometric cavity-assisted photothermal spectroscopy," Opt. Express **27**(9), 12183–12195 (2019).
21. M. Fox, *Quantum Optics: An Introduction* (Oxford University Press, 2006), Chap. 2.
22. P. C. D. Hobbs, "Ultrasensitive laser measurements without tears," Appl. Opt. **36**(4), 903–920 (1997).
23. G. Durry, I. Pouchet, N. Amarouche, T. Danguy, and G. Megie, "Shot-noise-limited dual-beam detector for atmospheric trace gas monitoring with near-infrared diode lasers," Appl. Opt. **39**(30), 5609–5619 (2000).
24. P. Werle, "A review of recent advantages in semiconductor laser based gas monitors," Spectrochim. Acta A **54**(2), 197–236 (1998).
25. F. L. Pedrotti, L. M. Pedrotti, and L. S. Pedrotti, *Introduction to Optics* 3rd Edition (Cambridge University Press, 2017), Chap. 8.
26. N. Hodgson and H. Weber, *Laser Resonators and Beam Propagation*, 2nd Edition (Springer) 2005, Part II.
27. R. Paschotta, H. R. Telle, and U. Keller, "Noise of Solid State Lasers," in *Solid-State Lasers and Applications* (CRC Press, 2007), Chap. 12.
28. I. E. Gordon, L. S. Rothman, C. Hill, R. V. Kochanov, Y. Tan, P. F. Bernath, M. Birk, V. Boudon, A. Campargue, K. V. Chance, B. J. Drouin, J.-M. Flaud, R. R. Gamache, J. T. Hodges, D. Jacquemart, V. I. Perevalov, A. Perrin, K. P. Shine, M.-A. H. Smith, J. Tennyson, G. C. Toon, H. Tran, V. G. Tyuterev, A. Barbe, A. G. Császár, V. M. Devi, T. Furtenbacher, J. J. Harrison, J.-M. Hartmann, A. Jolly, T. J. Johnson, T. Karman, I. Kleiner, A. A. Kyuberis, J.

Optics EXPRESS

Loos, O. M. Lyulin, S. T. Massie, S. N. Mikhailenko, N. Moazzen-Ahmadi, H. S. P. Müller, O. V. Naumenko, A. V. Nikitin, O. L. Polyansky, M. Rey, M. Rotger, S. W. Sharpe, K. Sung, E. Starikova, S. A. Tashkun, J. Vander Auwera, G. Wagner, J. Wilzewski, P. Wcisło, S. Yu, and E. J. Zak, "The HITRAN 2017 molecular spectroscopic database," J. Quant. Spectrosc. Radiat. Transfer **203**, 3–69 (2017).